Journal of Power Sources 266 (2014) 448–455

Contents lists available at ScienceDirect

Journal of Power Sources

journal homepage: www.elsevier.com/locate/jpowsour

# In situ electropolymerization of polyaniline/cobalt sulfide decorated carbon nanotube composite catalyst toward triiodide reduction in dye-sensitized solar cells

Yaoming Xiao [a, b, 1], Wei-Yan Wang [a, 1], Shu-Wei Chou [a], Tsung-Wu Lin [c], Jeng-Yu Lin [a, *]

[a] Department of Chemical Engineering, Tatung University, No. 40, Sec. 3, ChungShan North Rd., Taipei City 104, Taiwan
[b] Institute of Molecular Science, Key Laboratory of Chemical Biology and Molecular Engineering of Education Ministry, Shanxi University, Taiyuan 030006, PR China
[c] Department of Chemistry, Tunghai University, No. 181, Sec. 3, Taichung Port Rd., Taichung City 40704, Taiwan

## HIGHLIGHTS

- PANI/MWCNT@$CoS_{1.097}$ was synthesized using an in situ electropolymerization method.
- PANI/MWCNT@$CoS_{1.097}$ CE showed enhanced catalytic activity for $I_3^-$ reduction.
- The DSC with the PANI/MWCNT@$CoS_{1.097}$ CE reached an efficiency of 7.02%.

## GRAPHICAL ABSTRACT

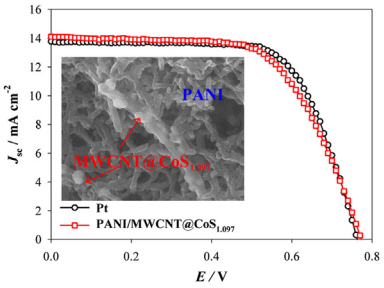


## ARTICLE INFO

*Article history:*
Received 11 March 2014
Received in revised form
25 April 2014
Accepted 11 May 2014
Available online 20 May 2014

*Keywords:*
Electropolymerization
Polyaniline
Cobalt sulfide
Carbon nanotube
Counter electrode
Dye-sensitized solar cell

## ABSTRACT

In this study, we report a composite film composed of the cobalt sulfide ($CoS_{1.097}$) nanoclusters/multiwall carbon nanotube nanocomposites (MWCNT@$CoS_{1.097}$) embedded polyaniline (PANI) film (denoted as PANI/MWCNT@$CoS_{1.097}$) by an in situ electropolymerization onto a fluorinated tin oxide (FTO) glass substrate as a counter electrode (CE) for Pt-free dye-sensitized solar cells (DSCs) for the first time. The extensive cyclic voltammograms (CVs) and electrochemical impedance measurements show the PANI/MWCNT@$CoS_{1.097}$ CE with an enhanced electrocatalytic activity for $I_3^-$ reduction compared to PANI and MWCNT@$CoS_{1.097}$ CEs. Moreover, the peak current densities of the PANI/MWCNT@$CoS_{1.097}$ CE show no sign of degradation after consecutive 200 CV tests, suggesting its great chemical and electrochemical stability. Furthermore, the DSC based on the in situ electropolymerized PANI/MWCNT@$CoS_{1.097}$ CE achieves an improved photovoltaic conversion efficiency of 7.02%, which is higher than those of the DSCs with PANI CE (6.06%) and with MWCNT@$CoS_{1.097}$ CE (5.54%), and is even comparable to that of the DSC using the Pt CE (7.16%). Therefore, the PANI/MWCNT@$CoS_{1.097}$ CE can be regarded as a promising alternative CE for Pt-free DSCs.



## 1. Introduction

Dye-sensitized solar cells (DSCs) based on a dye-sensitized nanocrystalline semiconductor anode, an electrolyte containing triiodide/iodide ($I_3^-/I^-$) redox couple and a Pt coated counter electrode (CE) have attracted widespread attentions as a promising

* Corresponding author. Tel.: +866 22592 5252x2561 119; fax: +866 22586 1939.
*E-mail addresses:* jylin@ttu.edu.tw, d923615@gmail.com (J.-Y. Lin).
[1] These authors contribute equally.

http://dx.doi.org/10.1016/j.jpowsour.2014.05.037
0378-7753/

alternative to conventional p–n junction solar cells due to their low cost, relatively high power conversion efficiency (PCE), and ease of fabrication [1–3]. As a crucial component in DSCs, the CE is functionalized to enable the transfer of electrons from the external circuit back to the $I_3^-$ species and catalyzes the reduction of $I_3^-$ to $I^-$ at the CE/electrolyte interface. Fluorine-doped tin oxide (FTO) glass substrate loaded with noble Pt is commonly used as the CE catalytic material due to its high conductivity, electrocatalytic activity and chemical stability [4,5]. However, in view of the scarce Pt resource, extensive attempts have been made to seek alternative CE materials, including carbon materials [6–8], conducting polymers [9–14], inorganic materials [15–19] the composites of the previous materials [20–37], and alloy compounds [38–40].

Among various conducting polymers, polyaniline (PANI) has attracted extensive research interests as one of the most promising candidates for noble Pt CE due to its exceptional electrochemical activity, high environmental stability and low cost. In additional to the electrocatalytic activity for $I_3^-$ reduction, the electrical conductivity of a non-Pt CE also plays a crucial role in determining the DSC performance. Biurdo and Viswanathan reported that PANI/graphite possessed an improved electrical conductivity compared with that without graphite, which can be ascribed to the formation of a highly conductive matrix by the conducting polymer around the graphite [34]. Thus, Huang et al. [21] successfully incorporated nanographite into the highly conducting PANI matrix as a composite CE. The DSC assembled with the composite CE achieved a PCE of 7.07%, up to 98% of that using a Pt CE. Furthermore, our group proposed a two-step method to prepare PANI/multi-wall carbon nanotube (MWCNT) composite CE via electrophoresis of MWCNTs onto an FTO substrate and then subjected to PANI electropolymerization [32]. The DSC based on the two-step synthesized PANI/MWCNT composite CE showed a significantly improved PCE of 6.24% compared to that of the DSCs with PANI or MWCNT CE.

On the other hand, MWCNT has been used as a potential alternative CE material owing to its highly specific surface, superior electronic conductivity, excellent mechanical strength and good chemical stability [41]. However, its intrinsically electrocatalytic activity for $I_3^-$ reduction is not satisfactory [26–32]. To achieve a comparable electrocatalytic activity to Pt CE, the surface of MWCNTs have decorated with several functional materials with the intrinsically high electrocatalytic activity. For instance, Li et al. [26] dispersed highly electrocatalytic TiN nanoparticles on the surface of MWCNTs, and obtained an improved electrocatalytic activity and photovoltaic performance. Song et al. [27] showed an enhanced PCE of 6.74% for the DSC with the MoN/MWCNT composite CE, which was much higher than that of the DSC using the MoN nanoparticle CE (5.57%). They claimed that the improvement is mainly attributed to a synergistic effect between the MoN nanoparticles and CNTs on ion diffusion and electrocatalysis. In additional to the transition metal nitrides, transition metal sulfides have recently acted as the electrocatalytic materials in DSCs. Our group synthesized a nanocomposite composed of few-layer $MoS_2$ nanosheets grown on the surface of MWCNTs [29]. The DSC assembled with the MWCNT@$MoS_2$ composite CE achieved a comparable PCE to that with Pt CE. Furthermore, we hydrothermally synthesized one-dimensional material composed of $CoS_{1.097}$ nanoclusters grown on the backbone of MWCNTs (denoted as MWCNT@$CoS_{1.097}$). It was observed that an enhanced PCE was achieved based on the MWCNT@$CoS_{1.097}$ composite catalytic film [30]. However; organic binders were still used in these studies to improve the adhesion with the FTO glass substrates, thus possibly resulting in the extra resistance in DSCs.

In this current work, we have successfully in situ electropolymerized PANI/MWCNT@$CoS_{1.097}$ composite catalyst toward $I_3^-$ reduction in dye-sensitized solar cells for the first time. Prior to the in situ electropolymerization, MWCNT@$CoS_{1.097}$ nanocomposites were synthesized via a facile hydrothermal method and aniline (ANI)/MWCNT@$CoS_{1.097}$ composites were then synthesized by a continuous reflux method. Owing to the lacking in the interconnections among the MWCNT@$CoS_{1.097}$ nanocomposites and the poor adhesion with the FTO glass substrate, the PANI conducting polymer network not only served a perfect conducting linker between the intrinsically electrocatalytic MWCNT@$CoS_{1.097}$ nanocomposites and the FTO glass substrate, but also provided a conducting matrix to facilitate electron transfer. When compared to the DSC assembled with the PANI or MWCNT@$CoS_{1.097}$ CE alone, the device using the in situ electropolymerized PANI/MWCNT@$CoS_{1.097}$ composite CE exhibited an enhanced electrocatalytic activity, thereby achieving an improved PCE of 7.02% to those of DSCs with the PANI CE and MWCNT@$CoS_{1.097}$ CE alone, which was even found to be comparable to that of a cell using a conventional sputtered Pt CE (7.16%).

## 2. Experimental

### 2.1. Fabrication of CEs

Firstly, MWCNT@$CoS_{1.097}$ nanocomposites were prepared by basically following our previous study [30]. In brief, the 30 mg acid-treated MWCNTs was added into an aqueous solution (60 mL) containing 0.05 M glucose and subjected to ultrasonication for 1 h to make a homogeneous dispersion. Then, 1.6 g of $CoCl_2 \cdot 6H_2O$ (98%, Acros), 5 g of thiourea was added into the MWCNTs suspension solution. After being stirred for 10 min, the precursor solution was transferred into a Teflon-lined stainless steel autoclave (150 mL). After assembling, the autoclave was heated at 110 °C for 4 h, followed by at 240 °C for 12 h and then cooled to room temperature. Finally, the precipitate was filtered off, washed with distilled water and dried at ambient atmosphere. The MWCNT@$CoS_{1.097}$ nanocomposites were further filtered by suction filtration, washed thoroughly with deionized water. It should be noted that the loading of $CoS_{1.097}$ on the MWCNTs was around 51 wt% as determined by using thermogravimetric analysis in our previous work [30].

Prior to the following preparation of CEs, the FTO glass substrates were first washed with a neutral cleaner, deionized water, acetone, and isopropanol by ultrasonication for 10 min, sequentially, and then treated with $O_2$ plasma (PDC-32G, HARRICK PLASMA) for 30 s to further clean the FTO surface. After that, the obtained MWCNT@$CoS_{1.097}$ nanocomposites were suspended in a 1:1 mixture of acetone and ethanol by ultrasonication for 2 h. Subsequently, the aqueous solution containing MWCNT@$CoS_{1.097}$ suspension in the concentration of 5.0 mg $mL^{-1}$ was drop-casted onto the cleaned FTO glass substrates (7 Ω $sq^{-1}$, NSG) and subjected to be dried at 50 °C for 30 min to obtain the MWCNT@$CoS_{1.097}$ CEs.

As for the PANI/MWCNT@$CoS_{1.097}$ CE, the ANI medium, containing 0.5 wt% of MWCNT@$CoS_{1.097}$ composites, was refluxed at 220 °C for 4 h to prepare the ANI/MWCNT@$CoS_{1.097}$ composites. The in situ electropolymerization of PANI/MWCNT@$CoS_{1.097}$ composite films onto cleaned FTO glass substrates were carried out using a Zahner electrochemical workstation (Zahner-Elektrik Gmbh & Co. KG, Germany) from a simple deposition bath (50 mL) containing 1.0 M ANI/MWCNT@$CoS_{1.097}$ composites and 2.0 M HCl in a three compartment cell, in which a cleaned FTO glass substrate and a Pt wire were employed as a working electrode and a counter electrode, respectively, in addition to a saturated silver/silver chloride (Ag/AgCl) reference electrode. The parameters for the in situ electropolymerization of PANI/MWCNT@$CoS_{1.097}$ CE were set with 1.3 V pulse-on potential, 0.2 V pulse-reversal potential, 1 s

pulse-on period, 0.5 s pulse-reversal period, and a total duration time of 150 s. The PANI CE was fabricated with the same pulse parameters in the aqueous consisting of ANI monomers alone. The obtained PANI MWCNT@$CoS_{1.097}$ and PANI CEs were rinsed with a diluted hydrochloric solution and distilled water, and then dried under a cool air flow. For comparison, ca. 100 nm thick of Pt layer was sputtered on an FTO glass substrate by means of a dc sputtering instrument (ULVAC) at a deposition rate of 0.28 nm $s^{-1}$.

### 2.2. Characterizations

The surface features of the PANI, MWCNT@$CoS_{1.097}$, and PANI/MWCNT@$CoS_{1.097}$ CEs were characterized using a field-emission scanning electron microscopy (FESEM; JSM-7600F). The crystal structure was explored by means of X-ray diffraction (XRD; Shimadzu Corporation) analysis. Fourier transform infrared spectra (FTIR) of samples were recorded on a Perkin Elmer Spectrum Gx FTIR Spectrometer using KBr as pellets. The cyclic voltammetry (CV) for $I^-/I_3^-$ system was conducted using a computer-controlled potentiostat (PGSTAT320N, Autolab) in the potential interval ranging from −0.4 V to 0.4 V vs. Pt at a scan rate of 10 mV $s^{-1}$. CV tests were performed in a 3-methoxypropionitrile solution composed of 50 mM LiI, 10 mM $I_2$, and 500 mM $LiClO_4$. During the CV tests, the as-prepared CE acted as the working electrode in a three-electrode one-compartment cell, in addition to a 4 $cm^2$ Pt sheet auxiliary electrode and a Pt wire reference electrode. The electrochemical impedance spectroscopy (EIS) measurements were carried out using the Zahner electrochemical workstation. The symmetric dummy cells were assembled for EIS studies. The detailed procedure for the fabrication of the symmetric dummy cell has been described elsewhere [21,31]. The impedance studies were carried out simulating open-circuit conditions at ambient atmosphere, and the impedance data covered a frequency range of $10^{-1}$–$10^6$ Hz with zero bias potential and 10 mV of amplitude, under a dark condition. The resultant impedance spectra were further analyzed using the Z-view software. The redox electrolyte consisting of 1 M 1,3-dimethylimidazolium iodide (Merck), 0.5 M 4-tert-butylpyridine (Aldrich), 0.15 M iodine (J.T. Baker), and 0.1 M guanidine thiocyanate (Aldrich) in 3-methoxypropionitrile (Acros) was employed for the EIS measurements.

### 2.3. Photoelectrochemical measurements

First, the cleaned FTO glass substrates were immersed in a bath of 40 mM solution of aqueous $TiCl_4$ at 70 °C for 30 min and subjected to be rinsed with deionized water, which can further improve the adhesion of the following prepared $TiO_2$ layer onto the FTO glass substrates. The 12 μm dense nanocrystalline $TiO_2$ layer (ETERDSC Ti-2105A, Eternal Chemical Co.) and 4 μm scattering $TiO_2$ layer (ETERDSC Ti-2325, Eternal Chemical Co.) were subsequently coated onto the FTO glass substrates by using a semiautomatic screen printer (ATMA, AT45PA), followed by gradually sintering under an air flow at 150 °C for 10 min, 325 °C for 5 min, 375 °C for 5 min, 450 °C for 15 min. The resulting $TiO_2$ photoanodes were further sensitized by immersing them into an ethanol solution consisting of 0.3 mM N719 dye (Everlight Chemical Industry Co.) at 40 °C for 4 h, followed by air drying. After dye adsorption, a $TiO_2$ photoanode was assembled with a CE. Then the electrolyte (aforementioned in the EIS testing electrolyte) was injected into the cell through the predrilled holes on the CE side. The photocurrent density–voltage characteristic was carried out using a computer-controlled Keithley 2400 source meter under illumination by a solar simulator (Yamashita Denso YSS-150A). During the measurements, the incident light intensity and the active cell area were controlled at 100 mW $cm^{-2}$ (AM 1.5) and 0.16 $cm^2$, respectively.

## 3. Results and discussion

Fig. 1 presents the top-view FE-SEM images of (a) bare FTO glass substrate, (b) PANI, (c) MWCNT@$CoS_{1.097}$, and (d) PANI/MWCNT@$CoS_{1.097}$ CEs. Compared to the bare FTO glass substrate, the morphology with the interconnected PANI nanofibers was

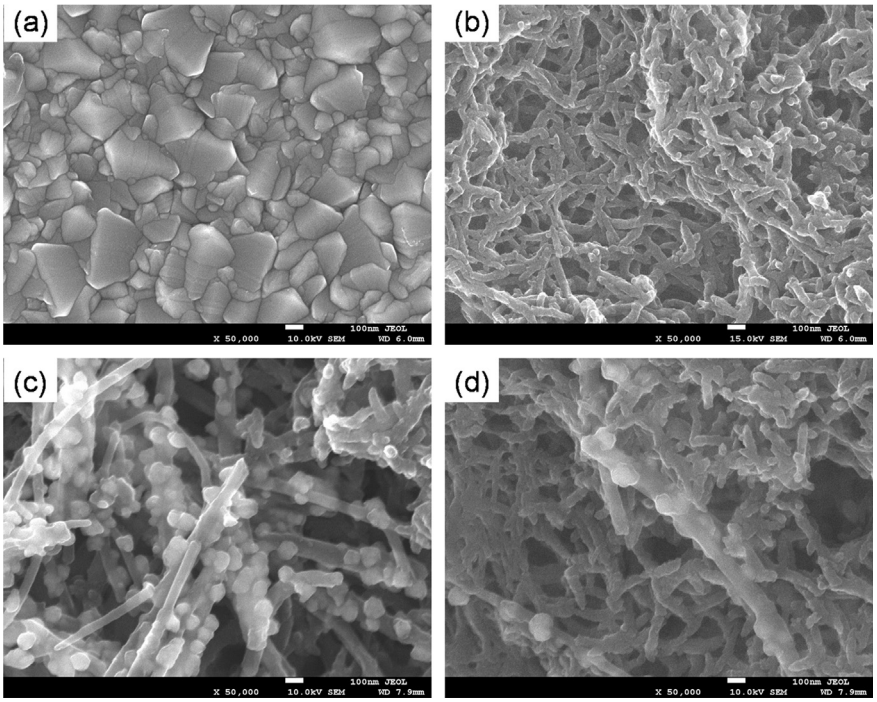


**Fig. 1.** FESEM images of the (a) FTO glass substrate, (b) PANI, (c) MWCNT@$CoS_{1.097}$, and (d) PANI/MWCNT@$CoS_{1.097}$ CEs.

presented for the PANI CE prepared by using the pulsed electropolymerization method. As for the MWCNT@$CoS_{1.097}$ CE, it can be found that the MWCNT@$CoS_{1.097}$ piled up on the FTO glass substrate with a weak adhesion. In order to utilize the excellent electrocatalytic activity of MWCNT@$CoS_{1.097}$ nanocomposites, it is necessary to improve the poor interconnections among the MWCNT@$CoS_{1.097}$ nanocomposites and the weak adhesion between the MWCNT@$CoS_{1.097}$ nanocomposites and the FTO glass substrate. Fig. 1d apparently shows that the MWCNT@$CoS_{1.097}$ nanocomposites were successfully incorporated into the highly conducting PANI matrix in the form as PANI/MWCNT@$CoS_{1.097}$ composite film on an FTO glass substrate after the in-situ electropolymerization.

To further identify the incorporation of MWCNT@$CoS_{1.097}$ into the conducting PANI matrix, XRD analyses were carried out. Fig. 2a presents the XRD pattern for the bare FTO glass substrate. Nevertheless, it is observed that the diffraction signals of PANI coated on an FTO glass substrate are almost the same with those presented for the FTO glass substrate except a weak broad peak at around 25°, suggesting the conducting PANI nanofibers possibly with the poor crystallization. It should be noted that the characteristic peak at around 25° can be ascribed to the (200) crystal orientation of PANI [42,43]. In addition, Fig. 2c displays the XRD pattern of the MWCNT@$CoS_{1.097}$ CE, in which three obvious diffraction peaks located at around 31°, 36°, and 48° can be indexed to the diffraction signals of $CoS_{1.097}$ [30,44]. In our previous study, we found that the diffraction intensity for the CNTs became much lower after highly covered with $CoS_{1.097}$ nanoclusters [30]. When the MWCNT@$CoS_{1.097}$ nanocomposites are loaded on the FTO substrate, the diffraction peaks from the MWCNTs is hardly observed according to the strong intensity from the FTO substrate. As for the XRD pattern of the PANI/MWCNT@$CoS_{1.097}$ CE, it illustrates the same diffraction peaks with those presented for the MWCNT@$CoS_{1.097}$ CE except the weak broad peak at around 25° originating from the PANI nanofibers. These results indicate most likely that the PANI/MWCNT@$CoS_{1.097}$ composite was successfully electropolymerized onto the FTO glass substrate.

To further examine the chemical composition of the composite, the FTIR analyses of the PANI, MWCNT@$CoS_{1.097}$, and PANI/MWCNT@$CoS_{1.097}$ were conducted and illustrated in Fig. 3. The

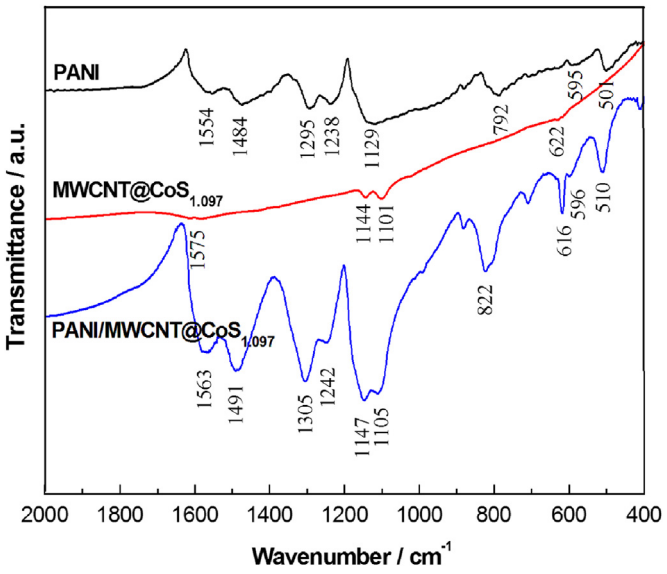


**Fig. 3.** FTIR spectra of PANI, MWCNT@$CoS_{1.097}$, and PANI/MWCNT@$CoS_{1.097}$.

characteristic absorption bands of the PANI nanofiber located at 1554 and 1484 $cm^{-1}$ can be attributed to the C=C stretching of quinoid ring and benzenoid deformation of PANI, respectively. The C–N stretching mode and bending mode are also observed at 1295 and 1238 $cm^{-1}$, respectively. Furthermore, the C–H bending of the quinoid ring at 1129 $cm^{-1}$ is found [22]. As can be seen in the MWCNT@$CoS_{1.097}$ curve, the absorption bands at 1575, 1144, and 1101 $cm^{-1}$ are associated with the stretching of the carbon nanotube backbone [45]. Notably, the spectrum of PANI/MWCNT@$CoS_{1.097}$ exhibits the combined vibrational bands illustrated in PANI and MWCNT@$CoS_{1.097}$ with little excursion. The FTIR spectra therefore indicate that the MWCNT@$CoS_{1.097}$ nanocomposites were successfully incorporated into the conducting PANI matrix, which is accordance with the findings from FESEM and XRD analyses.

To obtain insight into the reaction kinetics and electrocatalytic activities of the as-prepared PANI, MWCNT@$CoS_{1.097}$ and PANI/

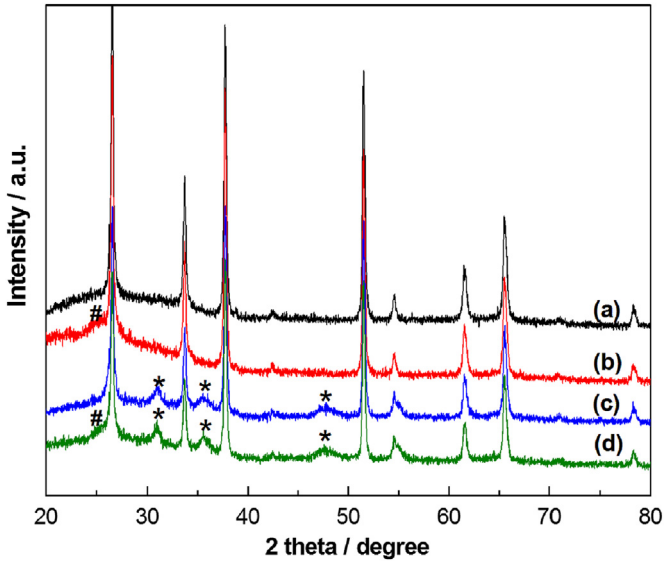


**Fig. 2.** XRD patterns of (a) FTO glass substrate, (b) PANI, (c) MWCNT@$CoS_{1.097}$, and (d) PANI/MWCNT@$CoS_{1.097}$ CEs. # and * indicate the diffraction peaks for PANI and $CoS_{1.097}$, respectively.

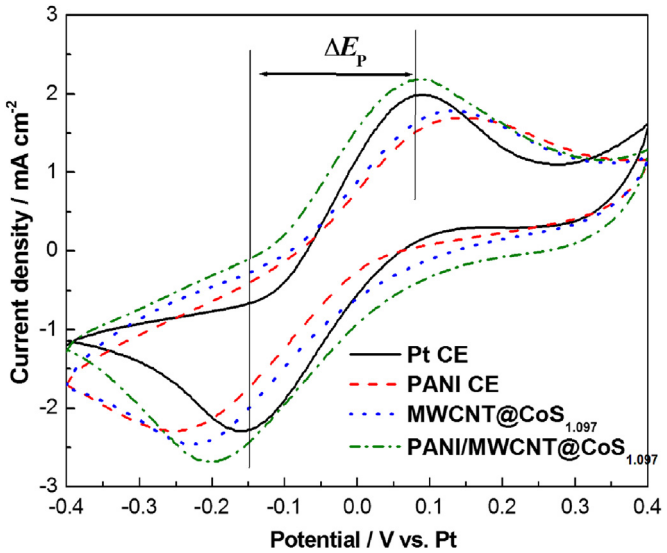


**Fig. 4.** CV curves of $I^-/I_3^-$ redox species for Pt, PANI, MWCNT@$CoS_{1.097}$, and PANI/MWCNT@$CoS_{1.097}$ CEs.

**Table 1**
Electrochemical parameters for various CEs.

| CE | $\Delta E_P$ (mV) | $R_S$ (Ω) | $R_T$ (Ω) | $Y_{CPE}$ (mF) | $R_{CT}$ (Ω) | $Z_N$ (Ω) |
|---|---|---|---|---|---|---|
| Pt | 250 | 13.81 | – | 0.19 | 2.47 | 3.89 |
| PANI | 401 | 17.02 | 2.46 | 1.41 | 3.67 | 9.79 |
| MWCNT@$CoS_{1.097}$ | 359 | 18.22 | 2.89 | 1.82 | 4.83 | 12.22 |
| PANI/MWCNT@$CoS_{1.097}$ | 289 | 17.31 | 2.64 | 2.37 | 3.02 | 7.92 |

MWCNT@$CoS_{1.097}$ CEs, CVs were carried out and the resultant CV curves are illustrated in Fig. 4. All CEs show a pair of oxidation and reduction peaks, the redox pair is attributed to the reaction of $I_3^- + 2e^- \leftrightarrow 3I^-$, which is directly related to the photovoltaic performance [46,47]. It is well known that the peak separation between the anodic and cathodic peaks, $\Delta E_P$, is inversely associated with the rate of the corresponding redox reaction [48]. The corresponding $\Delta E_P$ values for the aforementioned CEs are summarized in Table 1. As can be seen in Table 1, the significantly decreased $\Delta E_P$ is found when the MWCNT@$CoS_{1.097}$ composites are incorporated into the conducting PANI matrix. This is immediately responsible for the lower overpotential losses in the PANI/MWCNT@$CoS_{1.097}$ CE than PANI or MWCNT@$CoS_{1.097}$ CE. Furthermore, the PANI/MWCNT@$CoS_{1.097}$ CE presents the largest redox current densities among all CEs, signifying its larger active surface area for $I_3^-/I^-$ redox reaction. These can be due to its superior electrocatalytic activity from the MWCNT@$CoS_{1.097}$ nanocomposites and the highly conducting matrix from the PANI nanofibers structure. Fig. 5a shows 200 consecutive CV curves of the PANI/MWCNT@$CoS_{1.097}$ CE. In the consecutive 200-cycle CV tests, the redox current densities are increased at the first 30 CV cycles. However, the CVs do not change after 30 CV cycles possibly due to the fact that the electrolyte infiltrates into the PANI/MWCNT@$CoS_{1.097}$ film completely until 30 CV cycles. Additionally, the correlations between the redox peak current densities and the cycle numbers are summarized in Fig. 5b. After the first 30 cycles, both redox peak current densities retain stable with increasing the cycle number, even up to 200 cycles, signifying that the in situ electropolymerized PANI/MWCNT@$CoS_{1.097}$ composite film possesses excellent chemical and electrochemical stability [49].

To elucidate the electrocatalytic activities of the CEs for the reduction of $I_3^-$, EIS measurements were further performed. Fig. 6 represents the Nyquist plots obtained from various symmetric dummy cells composed of two identical CE materials. The intercept of the real axis at high frequency is the ohmic series resistance ($R_S$) including the sheet resistance of two identical CEs and the electrolytic resistance. The semicircle at high-frequency region refers to the charge-transfer resistance ($R_{CT}$) of the $I_3^-$ reduction at the redox electrolyte/CE interface, whereas the semicircle at low-frequency region represents the Nernst diffusion impedance ($Z_N$) corresponding to the diffusion resistance of the $I^-/I_3^-$ redox species in the bulk electrolyte. The constant phase element (CPE) is frequently used to describe deviation from the ideal capacitance due to the electrode surface roughness. It should be noted that the impedance of the carbon-based and polymer-based CE originating from the charge transport in the catalysts cannot be ignored, due to their relatively lower electrical conductivity compared with that of the Pt catalyst. Therefore, an element ($R_T$) representing the impedance for the charge transport resistance in the PANI, MWCNT@$CoS_{1.097}$ and PANI/MWCNT@$CoS_{1.097}$ films is introduced to the corresponding equivalent circuit [50]. Fig. S1a illustrates the equivalent circuit model employed to simulate the EIS spectrum of the Pt CE, while Fig. S1b represents the equivalent circuit models used to simulate the resultant EIS spectra of PANI, MWCNT@$CoS_{1.097}$, and PANI/MWCNT@$CoS_{1.097}$ CEs. The obtained impedance parameters are also summarized in Table 1. Interesting, it reveals a slightly lower $R_S$ value of 17.31 Ω for the PANI/MWCNT@$CoS_{1.097}$ CE compared to the MWCNT@$CoS_{1.097}$ CE (18.22 Ω). This can be ascribed to the fact that the incorporation of the conducting PANI matrix indeed improves the linkage among the MWCNT@$CoS_{1.097}$ nanocomposites, as well as the adhesion between the MWCNT@$CoS_{1.097}$ nanocomposites and the FTO glass substrate, thus resulting in improved charge transfer at the FTO/CE interface [23,24]. On the other hand, the $R_{CT}$, a direct measure of the electrocatalytic activity of a CE, can be calculated as half of the value obtained from the Z-view fitting owing to the symmetric configuration of the dummy cell. The $R_{CT}$ obtained for the PANI/MWCNT@$CoS_{1.097}$ CE (3.02 Ω) is relatively lower when compared to the PANI CE (3.67 Ω) and MWCNT@$CoS_{1.097}$ CE (4.83 Ω). This improvement can be attributed to the enhancement of the electrocatalytic activity via the incorporation of highly intrinsic electrocatalytic MWCNT@$CoS_{1.097}$ nanocomposites and the improvement of the linkage of MWCNT@$CoS_{1.097}$ nanocomposites and the adhesion between the MWCNT@$CoS_{1.097}$ nanocomposites and the FTO substrate by the conducting PANI matrix [23,24,51,52]. Thus, the PANI/MWCNT@$CoS_{1.097}$ CE prepared by the in situ electropolymerization shows comparable $R_{CT}$ value for $I_3^-$ reduction, as compared to the Pt CE (2.47 Ω). Moreover, the $Z_N$ arises from limitations in the mass transportation of the electrolyte, especially when considering its transport in the PANI, MWCNT@$CoS_{1.097}$ and PANI/MWCNT@$CoS_{1.097}$ thick films the diffusion length and resisting force of the electrolyte diffusion in the films were consequently increased, and thus $Z_N$ in these films cannot be ignored. It can be found that the PANI/MWCNT@$CoS_{1.097}$ CE had relatively lower $Z_N$ (7.92 Ω) compared with PANI (9.79 Ω) and MWCNT@$CoS_{1.097}$ (12.22 Ω) CEs. This also reveals that the incorporation of highly

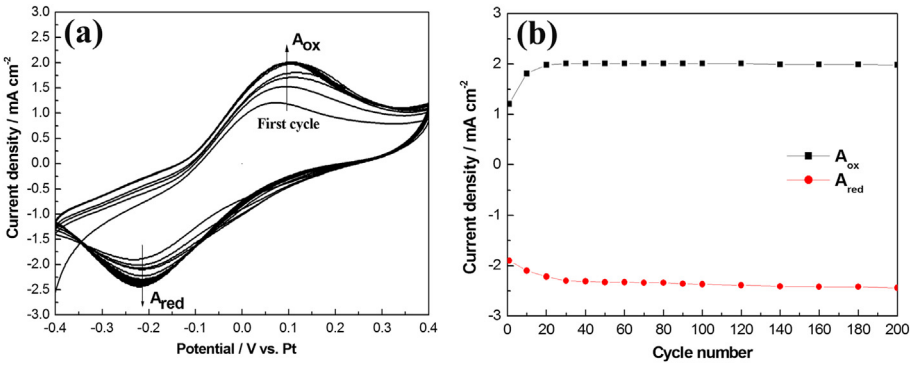


**Fig. 5.** (a) A total of 200 consecutive CVs for the $I_2/I^-$ system using the PANI/MWCNT@$CoS_{1.097}$ CE at a scan rate of 10 m $V^{-1}$, (b) the relationship between the cycle time and the redox peak current for the PANI/MWCNT@$CoS_{1.097}$ CE.

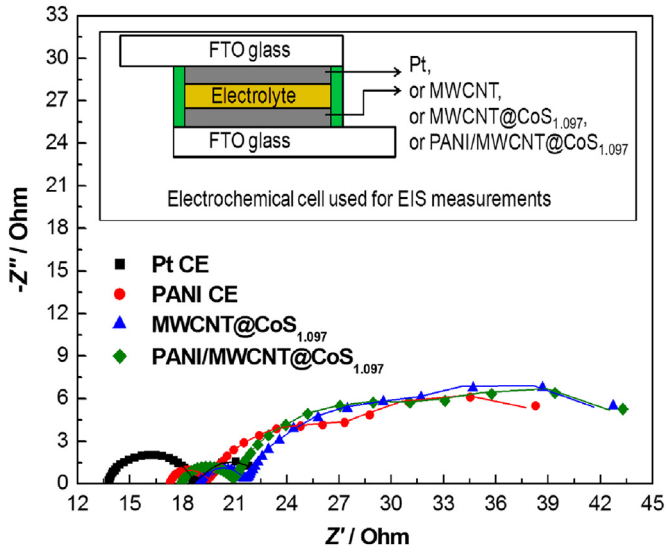


**Fig. 6.** Nyquist plots for the symmetrical cells assembled with Pt, PANI, MWCNT@$CoS_{1.097}$, and PANI/MWCNT@$CoS_{1.097}$ CEs.

electrocatalytic MWCNT@$CoS_{1.097}$ nanocomposites in the conducting PANI matrix with the abundant pores, which are able to shorten the ion diffusion path and facilitate ion diffusion transport. It should be noted that the CPE magnitude ($Y_{CPE}$) increases in the order of Pt (0.19 mF) < PANI (1.41 mF) < MWCNT@$CoS_{1.097}$ (1.82 mF) < PANI/MWCNT@$CoS_{1.097}$ (2.31 mF), suggesting the same tendency for the variance in active surface areas of the CEs [16]. This reveals that PANI/MWCNT@$CoS_{1.097}$ CE possesses a relatively higher active surface area for $I_3^-$ reduction, as confirmed by CV results.

Fig. 7 gives the photocurrent density–photovoltage curves of the DSCs based on Pt, PANI, MWCNT@$CoS_{1.097}$, and PANI/MWCNT@$CoS_{1.097}$ CEs. The corresponding values of short-circuit current density ($J_{SC}$), open-circuit voltage ($V_{OC}$), fill factor (FF), and cell efficiency ($\eta$) are summarized in Table 2. Notably, the DSCs based on Pt, PANI, and PANI/MWCNT@$CoS_{1.097}$ CEs have comparatively similar $V_{OC}$ value of 0.77 V. This is due to the $V_{OC}$ value is

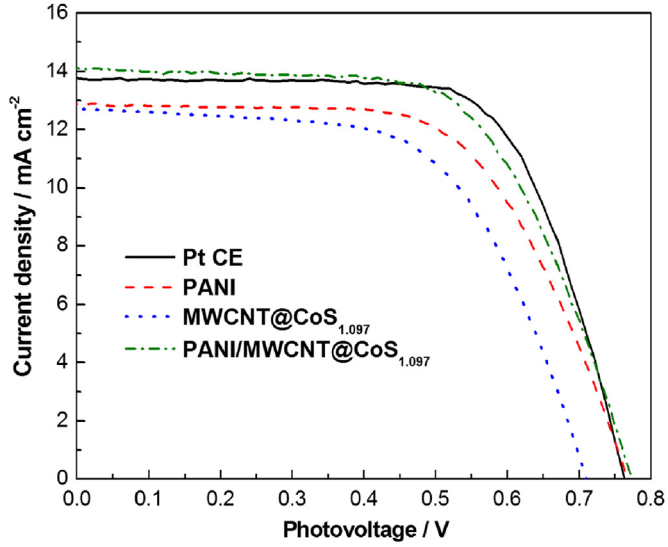


**Fig. 7.** Photocurrent density–voltage characteristics of the DSCs based on Pt, PANI, MWCNT@$CoS_{1.097}$, and PANI/MWCNT@$CoS_{1.097}$ CEs.

mainly determined by the energy level difference between the Fermi level of the electron in $TiO_2$ photoanode and the redox potential of the electrolyte [1,2], since these DSCs have the same components, their $V_{OC}$ values are therefore similar. Nevertheless, the poor interconnections between MWCNT@$CoS_{1.097}$ nanocomposites and the weak adhesion between the MWCNT@$CoS_{1.097}$ and the FTO glass substrate would reduce the electron transfer for the MWCNT@$CoS_{1.097}$ CE, thus leading to the DSC using the MWCNT@$CoS_{1.097}$ CE with poorer $V_{OC}$ (0.71) and FF values (0.59). The PANI CE provides better adhesion with the FTO glass substrate and thus the DSC based on the PANI CE offers relatively higher $V_{OC}$ (0.77), FF (0.62) and $\eta$ (6.06%) values. With regard to the DSC with the PANI/MWCNT@$CoS_{1.097}$ CE, the $\eta$ value is improved to 7.02%, much higher than PANI (6.06%) or MWCNT@$CoS_{1.097}$ (5.54%) based DSC. This improvement may be visually ascribed to the enhanced $J_{SC}$ and FF. This is because the intrinsically high electrocatalytic MWCNT@$CoS_{1.097}$ nanocomposites are incorporated into the conducting PANI matrix. Thus the increased active electrocatalytic sites from the MWCNT@$CoS_{1.097}$ nanocomposites and the faster electron-transfer pathway of PANI matrix enhance the $I_3^-$ reduction reaction and photogenerated electron-transfer at redox electrolyte/CE interface, as indicated in the CV and EIS tests [29,53–55]. Although the DSC assembled with the PANI/MWCNT@$CoS_{1.097}$ CE has a lower FF, it achieves a much higher $J_{SC}$, which resulted in a comparable photovoltaic performance at 100 mW $cm^{-2}$ illumination, with reference to the DSC using the Pt CE (7.16%). It should be noted that the mirror-like sputtered Pt CE has not only high electrocatalytic activity, but also high reflection of light to increase the inside of DSCs, thus enhancing the light-harvesting efficiency of DSCs [56]. With regard to the opaque PANI/MWCNT@$CoS_{1.097}$ CE, this effect is almost completely obstructed (Fig. S2). Fig. S3 further shows long-term stability result for the DSC assembled with the PANI/MWCNT@$CoS_{1.097}$ CE, in which the at-rest long-term stability data on the cell efficiency of the DSC were recorded each two days over a period of two weeks. It is found that the DSC based on the PANI/MWCNT@$CoS_{1.097}$ CE shows the reasonable stability in the long-term operation, which is also in consistence with the results from the aforementioned consecutive CV scans.

Finally, Fig. 8 shows the possible electrocatalytic mechanisms of PANI, MWCNT@$CoS_{1.097}$, and PANI/MWCNT@$CoS_{1.097}$ CEs toward $I_3^-$ reduction during the operation of the DSC. For the PANI CE, the PANI shows high conductivity and great adhesion with the FTO glass substrate, thus increasing lots of electron transport paths between the PANI and FTO glass. However, the PANI does not belong to the highly intrinsic electrocatalytic material because PANI generally has to possess sufficiently high active surface area to achieve a comparable electrocatalytic activity to conventional Pt CE. Although the MWCNT@$CoS_{1.097}$ CE has an obviously highly intrinsic electrocatalytic activity for $I_3^-$ reduction, only few electron transport paths are available between the MWCNT@$CoS_{1.097}$ nanocomposites and the MWCNT@$CoS_{1.097}$ nanocomposites and FTO glass substrate. To address this issue, the conducting PANI matrix in the PANI/MWCNT@$CoS_{1.097}$ composite film can not only serve as a catalyst but also as a conducting linker to connect the highly intrinsic electrocatalytic MWCNT@$CoS_{1.097}$ nanocomposites and improve the adhesion of MWCNT@$CoS_{1.097}$ nanocomposites

**Table 2**
Photovoltaic parameters for the DSCs based on various CEs.

| CEs | $J_{SC}$ (mA $cm^{-2}$) | $V_{OC}$ (V) | FF | $\eta$ (%) |
|---|---|---|---|---|
| Pt | 13.77 ± 0.12 | 0.77 ± 0.01 | 0.68 ± 0.01 | 7.16 ± 0.09 |
| PANI | 12.87 ± 0.22 | 0.77 ± 0.01 | 0.62 ± 0.01 | 6.06 ± 0.13 |
| MWCNT@$CoS_{1.097}$ | 12.73 ± 0.27 | 0.71 ± 0.02 | 0.59 ± 0.02 | 5.54 ± 0.28 |
| PANI/MWCNT@$CoS_{1.097}$ | 14.11 ± 0.16 | 0.77 ± 0.02 | 0.64 ± 0.01 | 7.02 ± 0.15 |

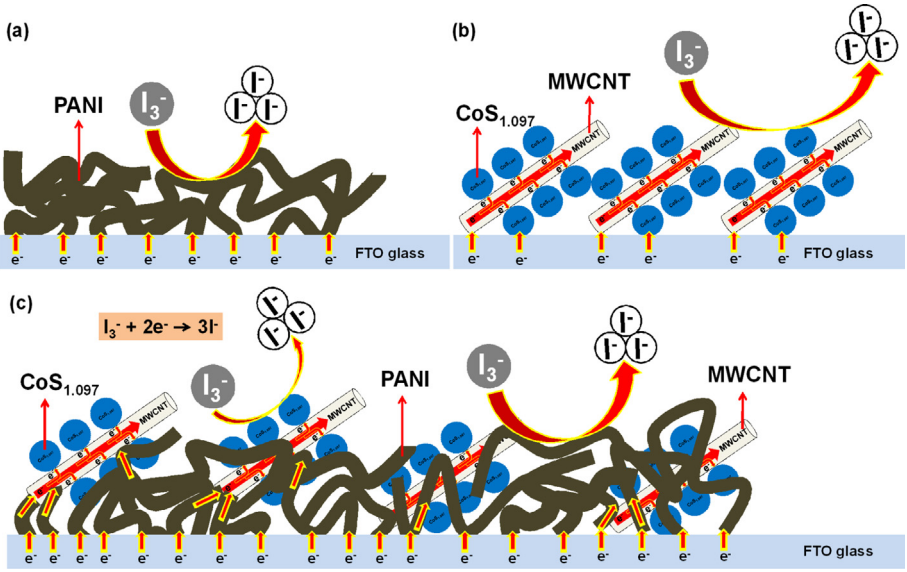


**Fig. 8.** Schematic of the electrocatalytic mechanisms of (a) PANI, (b) MWCNT@$CoS_{1.097}$, and (c) PANI/MWCNT@$CoS_{1.097}$ CEs, respectively.

with the FTO glass substrate. The MWCNT@$CoS_{1.097}$ nanocomposites, as highly active sites, demonstrate some dominant advantages to promote the fast $I_3^-$ reduction reaction. Moreover, the porous structure from the PANI nanofiber morphology and MWCNTs can facilitate the $I_3^-$ species diffusion. As a result, an apparent synergistic effect in the electrocatalytic activity for this composite CE can be expected.

## 4. Conclusions

In summary, highly electrocatalytic PANI/MWCNT@$CoS_{1.097}$ CE was successfully in situ electropolymerized onto the FTO glass substrate using a pulse potentiostatic electropolymerization method. The PANI/MWCNT@$CoS_{1.097}$ CE showed an enhanced excellent electrocatalytic activity for the $I_3^-/I^-$ redox reaction compared to PANI CE and MWCNT@$CoS_{1.097}$ CE due to the interconnect between the highly intrinsic electrocatalytic MWCNT@$CoS_{1.097}$ nanocomposites and the improvement of the adhesion of MWCNT@$CoS_{1.097}$ nanocomposites with the FTO glass substrate by implement of the conducting PANI matrix. The light-to-electric energy conversion efficiency of this Pt-free DSC reached 7.02%, which is up to 95% of that of the DSC based on the conventional Pt CE under full sunlight illumination (100 mW $cm^{-2}$, AM 1.5 G). Therefore, the PANI/MWCNT@$CoS_{1.097}$ CE prepared by the in situ electropolymerization technique shows a great potential as a low-cost alternative capable of noble Pt CE for large-scale DSCs.

## Acknowledgment

This research was supported by Ministry of Science and Technology in Taiwan under contracts NSC-101-2221-E-036-035 and MOST 103-3113-M-110-001.

## Appendix A. Supplementary data

Supplementary data related to this article can be found at http://dx.doi.org/10.1016/j.jpowsour.2014.05.037.

## References

[1] B. O'Regan, M. Grätzel, Nature 353 (1991) 737–740.
[2] M. Grätzel, Inorg. Chem. 44 (2005) 6841–6851.
[3] H.C. Weerasingle, F. Huang, Y.B. Cheng, Nano Energy 2 (2013) 174–189.
[4] M. Grätzel, Nature 414 (2001) 338–344.
[5] A. Hagfeldt, G. Boschloo, L. Sun, L. Kloo, H. Pettersson, Chem. Rev. 110 (2010) 6595–6663.
[6] A. Kay, M. Grätzel, Sol. Energy Mater. Sol. Cells 44 (1996) 99–117.
[7] E. Ramasamy, W.J. Lee, D.Y. Lee, J.S. Song, Electrochem. Commun. 10 (2008) 1087–1089.
[8] G. Veerappan, K. Bojan, S.W. Rhee, ACS Appl. Mater. Interfaces 3 (2011) 857–862.
[9] J.M. Pringle, V. Armel, D.R. MacFarlane, Chem. Commun. 46 (2010) 5367–5369.
[10] K.S. Lee, H.K. Lee, D.H. Wang, N.G. Park, J.Y. Lee, O.O. Park, J.H. Park, Chem. Commun. 46 (2010) 4505–4507.
[11] T. Muto, M. Ikegami, T. Miyasaka, J. Electrochem. Soc. 157 (2010) B1195–B1200.
[12] Q. Li, J. Wu, Q. Tang, Z. Lan, P. Li, J. Lin, L. Fan, Electrochem. Commun. 10 (2008) 1299–1302.
[13] S. Ameen, M.S. Akhtar, Y.S. Kim, O.B. Yang, H.S. Shin, J. Phys. Chem. C 114 (2010) 4760–4764.
[14] Y. Xiao, J.Y. Lin, J. Wu, S.Y. Tai, G. Yue, Electrochim. Acta 83 (2012) 221–226.
[15] M.K. Wang, A.M. Anghel, B. Marsan, N.C. Ha, N. Pootrakulchote, S.M. Zakeeruddin, M. Grätzel, J. Am. Chem. Soc. 131 (2009) 15976–15977.
[16] M.X. Wu, Y.D. Wang, X. Lin, N. Yu, L. Wang, A. Hagfeldt, T.L. Ma, Phys. Chem. Chem. Phys. 13 (2011) 19298–19301.
[17] G.R. Li, J. Song, G.L. Pan, X.P. Gao, Energy Environ. Sci. 4 (2011) 1680–1683.
[18] J.Y. Lin, J.H. Liao, S.W. Chou, Electrochim. Acta 56 (2011) 8818–8826.
[19] H.C. Sun, D. Qin, S.Q. Huang, X.Z. Guo, D.M. Li, Y.H. Luo, Q.B. Meng, Energy Environ. Sci. 4 (2011) 2630–2637.
[20] B. He, Q. Tang, J. Luo, Q. Li, X. Chen, H. Cai, J. Power Sources 256 (2014) 170–177.
[21] K.C. Huang, J.H. Huang, C.H. Wu, C.Y. Liu, H.W. Chen, C.W. Chu, J.T. Lin, C.L. Lin, K.C. Ho, J. Mater. Chem. 21 (2011) 10384–10389.
[22] G. Wang, W. Xing, S. Zhou, Electrochim. Acta 66 (2012) 151–157.
[23] M.H. Yeh, L.Y. Lin, C.P. Lee, H.Y. Wei, C.Y. Chen, C.G. Wu, R. Vittal, K.C. Ho, J. Mater. Chem. 21 (2011) 19021–19029.
[24] C.T. Li, C.P. Lee, Y.Y. Li, M.H. Yeh, K.C. Ho, J. Mater. Chem. A 1 (2013) 14888–114896.
[25] P. Sudhagar, S. Nagarajan, Y.G. Lee, D. Song, T. Son, W. Cho, M. Heo, K. Lee, J. Won, Y.S. Kang, ACS Appl. Mater. Interfaces 3 (2011) 1838–1843.
[26] G.R. Li, Q.W. Jiang, X.P. Gao, P.W. Shen, Angew. Chem. Int. Ed. 49 (2010) 3653–3656.
[27] J. Song, G.R. Li, F.X. Xiong, X.P. Gao, J. Mater. Chem. 22 (2012) 20580–20585.
[28] B. He, Q. Tang, M. Wang, C. Ma, S. Yuan, J. Power Sources 256 (2014) 8–13.
[29] S.Y. Tai, C.J. Liu, S.W. Chou, F.S.S. Chien, J.Y. Lin, T.W. Lin, J. Mater. Chem. 22 (2012) 24753–24759.
[30] J.Y. Lin, S.Y. Tai, S.W. Chou, J. Phys. Chem. C 118 (2014) 823–830.
[31] J.Y. Lin, J.H. Liao, T.Y. Hung, Electrochem. Commun. 13 (2011) 977–980.
[32] Y. Xiao, J.Y. Lin, J. Wu, S.Y. Tai, G. Yue, T.W. Lin, J. Power Sources 233 (2013) 320–325.
[33] J.Y. Lin, C.Y. Chan, S.W. Chou, Chem. Commun. 49 (2013) 1440–1442.
[34] S.E. Biurdo, T. Viswanathan, Carbon 43 (2005) 2983–2988.
[35] B. He, Q. Tang, T. Liang, Q. Li, J. Mater. Chem. A 2 (2014) 3119.

[36] Q. Tang, H. Cai, S. Yuan, X. Wang, J. Mater. Chem. A 1 (2013) 317.
[37] M. Wang, Q. Tang, H. Chen, B. He, Electrochim. Acta 125 (2014) 510.
[38] F. Gong, H. Wang, X. Xu, G. Zhou, Z.S. Wang, J. Am. Chem. Soc. 134 (2012) 10953.
[39] B. He, X. Meng, Q. Tang, P. Li, S. Yuan, P. Yang, J. Power Sources 260 (2014) 185.
[40] H. Cai, Q. Tang, B. He, P. Li, J. Power Sources 258 (2014) 117.
[41] C.E. Banks, R.G. Compton, Analyst 131 (2006) 15–21.
[42] D. Kim, J. Choi, J.Y. Kim, Y.K. Han, D. Sohn, Macromolecules 35 (2002) 5314–5316.
[43] X. Sui, Y. Chu, S. Xing, M. Yu, C. Liu, Colloids Surf. A 251 (2004) 103–107.
[44] Q. Wang, L. Jiao, H. Du, J. Yang, Q. Huan, W. Peng, Y. Si, Y. Wang, H. Yuan, CrystEngComm 13 (2011) 6960–6963.
[45] T. Saleh, S. Agarwal, V. Gupta, Appl. Catal. B Environ. 106 (2011) 46–53.
[46] X. Mei, S. Cho, B. Fan, J.Y. Ouyang, Nanotechnology 21 (2010) 395202–395210.
[47] Z. Huang, X.Z. Liu, K.X. Li, D.M. Li, Y.H. Luo, H. Li, W.B. Song, L.Q. Chen, Q.B. Meng, Electrochem. Commun. 9 (2007) 596–598.
[48] J. Roy-Mayhew, D. Bozym, C. Punckt, I. Aksay, ACS Nano 4 (2010) 6203–6211.
[49] H. Guo, Y. Li, L. Fan, X. Wu, M. Guo, Electrochim. Acta 51 (2006) 6230–6237.
[50] J. Chen, B. Li, J. Zheng, J. Zhao, H. Jing, Z. Zhu, Electrochim. Acta 56 (2011) 4624–4630.
[51] A. Fujiwara, Y. Matsuoka, Y. Matsuoka, H. Suematsu, N. Ogawa, K. Miyano, H. Kataura, Y. Maniwa, S. Suzuki, Y. Achiba, Carbon 42 (2004) 919–922.
[52] G. Mor, K. Shankar, M. Paulose, O. Varghese, C. Grimes, Nano Lett. 6 (2006) 215–218.
[53] Y. Saito, W. Kubo, T. Kitamura, Y. Wada, S. Yanagida, J. Photochem. Photobiol. A 164 (2004) 153–157.
[54] J.Y. Lin, J.H. Liao, J. Electrochem. Soc. 159 (2012) D65–D71.
[55] E. Ramasamy, W.J. Lee, D.Y. Lee, J.S. Song, J. Power Sources 165 (2007) 446–449.
[56] X. Fang, T. Ma, G. Guan, M. Akiyama, T. Kida, E. Abe, J. Electroanal. Chem. 570 (2004) 257–263.